# Mean velocity and length-scales in the overlap region of wall-bounded turbulent flows

Yoshinori Mizuno[a] and Javier Jiménez[b]
*School of Aeronautics, Universidad Politécnica de Madrid, 28040 Madrid, Spain*

The length scales of the spectra and correlation functions of the velocity fluctuations in the overlap region of turbulent wall-bounded flows are analyzed. It is found that a mixing length based on the mean local shear works better as a normalization than the distance to the wall. To define an overlap range sufficiently long and independent of the Reynolds number to allow the two scalings to be tested, the classical asymptotic expansion of the mean shear is extended to include a near-wall virtual origin and a wake component. The result represents well the velocity profile in $y^+ > 70$ and $y/\delta < 0.3 - 0.5$ for $Re_\tau \gtrsim 2000$, and the spectral scales for $Re_\tau \gtrsim 500$. It is suggested that the scaling with a local mixing length could be interpreted as an indication that the size of the eddies is more related to the local shear time scale than to the interaction with the wall. It is also noted that the linearity of the mixing length is a more robust indicator of a logarithmic regime than those that rely on a zero virtual origin. © *2011 American Institute of Physics*. [doi:10.1063/1.3626406]

## I. INTRODUCTION

One of the most characteristic features of wall-bounded turbulence is the inhomogeneity of the length-scales of the velocity fluctuations. They are small near the wall, where they scale in the wall units defined by the friction velocity $u_\tau$ and by the kinematic viscosity $\nu$, and larger in the outer layers, where they are determined by the flow geometry. In the intermediate region, where the distance, $y$, from the wall is large in wall units but small with respect to the flow thickness, there is no obvious unit of length, and it has been customary to use $y$ for that purpose.[1] Conceptually, there are other possibilities. An obvious one is the mixing length formed with the global velocity scale, $u_\tau$, and the inverse of the local shear,

$$l(y) = \left( \frac{1}{u_\tau} \frac{dU}{dy} \right)^{-1},\qquad(1)$$

where $U$ is the mean streamwise velocity. Other choices can be found in the turbulence-modeling literature. For high enough Reynolds numbers, Townsend[2] hypothesized that structures away from the wall are self-similar with respect to $y$, independently of the viscosity and of the wall roughness, so that

$$l \propto y.\qquad(2)$$

The well-known logarithmic law follows from integrating Eq. (2). If the superscript "$+$" is used for variables normalized in wall units,

$$U^+ = \frac{1}{\kappa_0} \log\, y^+ + B_0,\qquad(3)$$

where $\kappa_0$ is the Kármán constant and the intercept $B_0$ depends on the properties of the wall.

In ideal circumstances, all the length scales in the overlap region should be proportional to each other, because the mean profile is determined by whatever is the controlling scale. On the other hand, Eqs. (1) and (2) reflect different physics. While Eq. (2) suggests the attached-eddy hypothesis that the growth of the energy-containing structures is controlled by their interactions with the wall,[3] Eq. (1) emphasizes the deformation caused by the local shear. Moreover, it is in non-ideal situations, where Eq. (3) is not exactly satisfied, that the two physical models can be distinguished more readily. The purpose of the present paper is to take advantage of the discrepancies between ideal and non-ideal behaviors to explore the scaling characteristics of the flow in the overlap region between the inner and outer layers.

We represent by $x$, $y$, and $z$ the streamwise, wall-normal, and spanwise coordinates, and by $u$, $v$, and $w$ the corresponding velocity components. The friction Reynolds number is $Re_\tau \equiv \delta^+$, where $\delta$ is the pipe radius, the channel half-height, or the 99% boundary-layer thickness.

The behavior of the length-scales of the velocity fluctuations has been studied extensively. Only the intermediate scales of the two-point correlations of the streamwise velocity grow approximately linearly with $y$.[4,5] The smaller eddies scale in Kolmogorov's viscous units. The larger ones reach from the outer region to the wall without changing their sizes, scale with $\delta$, and lead to anomalous intensities of the near-wall fluctuations.[6,7] The larger eddies have been classified into large-scale motions (LSMs), with sizes that do not exceed a few boundary layer thicknesses, and very large-scale ones (VLSMs), specially of the streamwise velocity, which are much longer. It is typically only the hierarchy of eddies leading to the LSMs that scale with the wall distance.[8–10] For example, Ref. 10 finds that the azimuthal dimensions of those eddies increase linearly with $y$ in pipes, while those of VLSMs grow more slowly. The spanwise length-scale of the streamwise velocity fluctuations also grows linearly in channels[11,12] and in boundary layers,[13] and

[a]Present address: Department of Mechanical and Aerospace Engineering, Monash University, VIC 3800, Australia.
[b]Also at Centre for Turbulence Research, Stanford University, Stanford, California 94305, USA.

is robust against wall disturbances.[14] The two-point correlations and spectra of the wall-normal velocity, which are less contaminated by large eddies, always scale more closely with $y$ than those of the streamwise velocity.[7,15–17]

Those observations suggest that Eq. (2) needs corrections in real flows. In fact, even when it holds, the origin of the linear scaling does not always coincide with the wall, and Eq. (2) has to include a non-zero virtual origin,

$$l \propto (y - y_{off}). \qquad (4)$$

For example, it is common to adjust the reference position of $y$ in flows over rough walls,[18] in the same way as virtual origins are used in self-similar shear layers or jets. Those adjustments are typically required whenever different physics separates the origin from the self-similar domain, and there is no reason to exclude them for smooth walls, where self-similarity only holds above the viscous near-wall layer. In the context of the logarithmic law for $U$, which follows from either Eq. (2) or Eq. (4), Ref. 19 postulates an offset from physical considerations, and the Lie-group analysis of the Navier-Stokes equations explicitly allows one.[20] Reference 21 estimated it to be $y_{off}^+ = 8$ for pipes and channels in the range $Re_\tau = 180$ to $53\,000$. An offset $y_{off}^+ = -7.5$ was found to represent best the logarithmic mean velocity profile in numerical Ekman layers,[22] and a mixing-length theory incorporating $y_{off}^+ = -8.2$ has been shown to predict the mean velocity of boundary layers well below the classical overlap region.[23]

In fact, it turns out that the local mixing length in Eq. (1), which generally includes both an offset and other corrections, scales the velocity spectra better than $y$. Defining the spectrum,

$$\phi_{\zeta\zeta}(y, \lambda_x, \lambda_z) \equiv \langle \hat{\zeta}(y, \lambda_x, \lambda_z) \hat{\zeta}^*(y, \lambda_x, \lambda_z) \rangle,$$

where $\zeta$ is an arbitrary velocity component, $\hat{\zeta}$ is its Fourier transform, the asterisk stands for complex conjugation, and $\langle \rangle$ denotes ensemble averaging. The wavelengths are defined as $\lambda = 2\pi/k$, in terms of the wavenumbers $k$. Figure 1 shows the premultiplied spectra of the streamwise and wall-normal velocities in the overlap layer of a channel flow with $Re_\tau = 934$,[7] comparing the normalization using the length in Eq. (1) with the purely linear one using $y$. It is clear that the former is better than the latter. Note that the relatively low Reynolds number of that figure is chosen on purpose, as explained above. For a channel with $Re_\tau = 2003$,[24] a better collapse is also obtained using $l(y)$, but the difference is less marked, because corrections from the inner and outer regions are smaller. The contour levels in Fig. 1 are chosen relatively intense to isolate the energetic modes in the spectral cores. Lower contours do not collapse as well in either scaling, because they include smaller and larger eddies that we have already seen to behave differently. Even at these contour levels, the smallest scales collapse only moderately with $l(y)$, although much better than with $y$.

Note that any model for $l(y)$ must take into account the outer corrections traditionally expressed as a "wake" function,[31] which depend on the Reynolds number and on the flow geometry. For example, the linear scaling in Eq. (2) is harder to observe in boundary layers than in channels,[17] because of the stronger wake in the former. That difference is believed to persist at all Reynolds numbers.
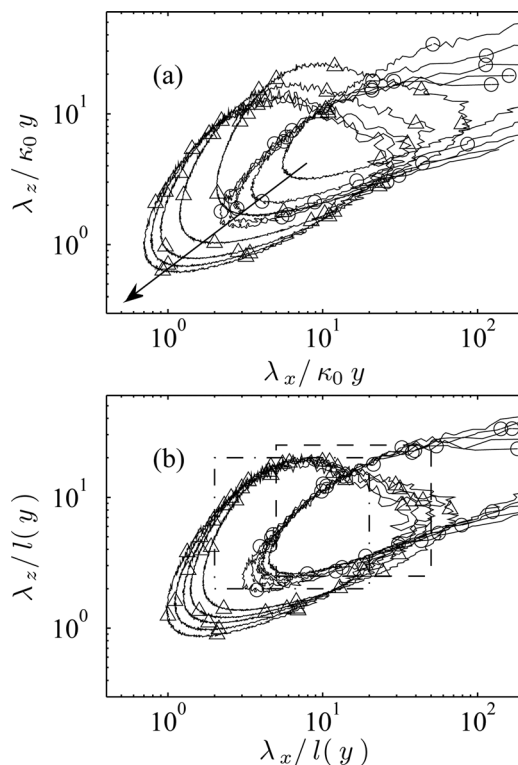


FIG. 1. Premultiplied two-dimensional spectra of the velocity fluctuations, as functions of the wavelengths. (a) Normalized with $\kappa_0 y$, where $\kappa_0 = 0.365$. (b) Normalized with $l(y)$ from Eq. (1). Channel C3 at $Re_\tau = 934$.[7] ○, $k_x k_z \phi_{uu}$; △, $k_x k_z \phi_{vv}$. Contours are 0.05 of the local mean-squared intensity of each component. Spectra are shown at $y/\delta = 0.1, 0.15, 0.2, 0.3,$ and 0.4, with the arrow in the direction of increasing $y$. The rectangles enclose the "core" ranges defined in: — —, Eq. (12) for $u$; — · —, Eq. (13) for $v$.

Incorporating into the logarithmic law, a more complicated scale dependence than the usual linear one has some practical consequences. For example, if the logarithmic profile is used to estimate $u_\tau$, an error in the origin implies an error in the estimated friction and in the location of the whole profile. Moreover, the logarithmic law (3) and the linear assumption (2) are key ingredients in many models of the inner region used in RANS or LES, where they enter as off-wall boundary conditions.[32] They require corrections, if the logarithmic law is generalized.

This paper is organized in two parts. Section II inquires into how much the mixing length deviates from $y$ in real flows, introduces a model for the differences between $l(y)$ and the pure linear scaling, and calibrates it using numerical and experimental data. That allows us to estimate $l(y)$ even when the data is too noisy or too sparse to compute derivatives and to give uniform limits for the extent of the asymptotic overlap region. Section III uses $l(y)$ to test the behavior of both wall-parallel and wall-normal velocity length-scales, and the conclusions are summarized in Sec. IV.

## II. A MODEL FOR THE LENGTH-SCALE

### A. Shifted model with a wake

Our first task is to determine whether it is possible to extend the overlap scaling of the mean velocity profile to a region that is reasonably independent of the Reynolds

number, or at least whose dependence on $Re_\tau$ can be predicted. That implies extending the definition of the overlap profile, in a manner similar to those in Refs. 33–36.

The logarithmic profile of $U$ follows from the linear assumption in Eq. (2), but, from the point of view of asymptotic analysis, it is the lowest-order approximation of an asymptotic expansion in the small parameter $\varepsilon \equiv Re_\tau^{-1}$. The inner expansion of the velocity gradient is a function of $y^+$, and the outer one is a function of $\eta \equiv \varepsilon y^+ = y/\delta$. For pipes and channels, matching the two expansions in the region where $y^+ \gg 1$ and $\eta \ll 1$ results in the overlap profile,[33–36]

$$\frac{dU^+}{dy^+} = \frac{\kappa_0^{-1} + \varepsilon a_1}{y^+} + \frac{d_0 + \varepsilon d_1}{y^{+2}} + \varepsilon e_2 \eta + O(\varepsilon^2), \quad (5)$$

where, we have omitted terms that will turn out to be zero, and higher-order ones of the form $\eta^n$ for $n > 1$ and $1/y^{+n}$ for $n > 2$. A similar form is obtained for boundary layers.[37,38] The variables used in Eq. (5) recognize that the positive powers of $\eta$ belong to the inner expansion of the outer wake of the velocity profile, while the negative powers of $y^+$, which are dominant near the wall, are part of the inner profile. Since

$$\frac{1}{y^+ - y_{off}^+} = \frac{1}{y^+} + \frac{y_{off}^+}{y^{+2}} + O(1/y^{+3}),$$

the $1/y^{+2}$ term in Eq. (5) can be incorporated, for $y^+ \gg 1$, into a virtual origin for $y$ in the logarithm in Eq. (3), where $y_{off}$ can be expected to scale in wall units. The shifted linear scaling in Eq. (4) is equivalent to Eq. (5) to $O(\varepsilon)$.

The resulting approximation is

$$\frac{dU^+}{dy^+} \approx \frac{1}{\kappa(y^+ - y_{off}^+)} + \frac{e_2}{Re_\tau}\eta, \quad (6)$$

where $\kappa^{-1} = \kappa_0^{-1} + \varepsilon a_1$ and $y_{off}^+ = \kappa(d_0 + \varepsilon d_1)$. The functional form of the last term in Eq. (6) is chosen to be consistent with the traditional representation of the mean velocity as a composite profile of the form,[31]

$$U^+ = \frac{1}{\kappa}\log y^+ + B + \frac{\Pi}{\kappa}W(\eta), \quad (7)$$

with a wake that is quadratic near the wall,[39]

$$W(\eta) = 2\eta^2(3 - 2\eta) - \Pi^{-1}\eta^2(1 - 3\eta + 2\eta^2). \quad (8)$$

The rightmost term in Eq. (6) is the leading-order expansion of Eq. (8) and is related to the wake parameter by $e_2 = 2(6\Pi - 1)/\kappa$. We will only use $\Pi$ from now on. Note that the form of the expansions in Eq. (5) suggests that the parameters $\kappa$, $y_{off}^+$, and $\Pi$, might depend approximately on the Reynolds number as $\beta + \alpha/Re_\tau$, where $\alpha$ and $\beta$ are constants to be determined later.

Viscous effects are modeled by a virtual origin for $y$,[21] and outer ones by the additional term corresponding to the profile "wake." The scaling of the mean velocity profile has been discussed extensively, and even the validity of the logarithmic law has been questioned,[40] but our main interest here is whether the mean profile describes the scaling of the ge-

ometry of the velocity fluctuations better than the distance to the wall. The purpose of this section is to determine how an expression such as Eq. (6), which can still be considered as an intermediate asymptotic expansion, can be used to extend the range of the self-similar region beyond that of the basic logarithmic approximation.

## B. Calibration

To calibrate the parameters in Eq. (6), we minimize, for each of the data sets in Table I, the cost function,

$$S^2(y_l, y_u; \boldsymbol{q}) \equiv \frac{1}{y_n - y_0}\sum_{i=1}^{n}\left[\frac{l_i^+ - m^+(y_i; \boldsymbol{q})}{y_i^+}\right]^2(y_i - y_{i-1}), \quad (9)$$

where the $y_i$ are the positions of the available data and $y_l < y_1 < \cdots < y_n < y_u$. The choice of the fitting interval $(y_l, y_u)$ is discussed below. The model corresponding to Eq. (6) is

$$m^+(y; \boldsymbol{q}) \equiv \left[\frac{1}{\kappa(y^+ - y_{off}^+)} + \frac{2(6\Pi - 1)}{\kappa Re_\tau^2}y^+\right]^{-1}, \quad (10)$$

and the parameters to be adjusted are $\boldsymbol{q} \equiv (\kappa, y_{off}, \Pi)$. The point $y_0$, which is needed for the integration in Eq. (9), is the last data point below the lower end of the fitting interval, $y_l$. Since the range of validity of the model is unknown a-priori, we use the Levenberg–Marquardt damped least squares iterative algorithm[41] to optimize the parameters for all the possible values of $y_l$ and $y_u$.

Figures 2(a) and 2(b) show contours of the resulting optimal $\kappa$ and $\Pi$ for the numerical channel C4, as functions of the limits of the fitting interval. The corresponding optimum values of the cost function $S$ are given in Fig. 2(c), which has several local minima corresponding to fits to different parts of the velocity profile. However, there is a clear region of relatively small errors, bounded by $y_l^+ \gtrsim 100$ and $y_u^+ < 1100$, at whose lower-right corner there is a local minimum that we take as the longest possible asymptotic fit. This location is marked by a cross in the plots. It falls within relatively uniform plateaus in which the parameters $\kappa$, $\Pi$ (and $y_{off}$, not shown here) vary only weakly with $y_l$ and $y_u$. This can be interpreted to mean that the model (10), with the parameters at the local minimum, fits the velocity profile in the range of wall distances given by $y_l$ and $y_u$. The same procedure was applied to all the other data sets, although some of the experimental profiles had to be interpolated to denser grids using cubic splines to obtain a smooth behavior of the fitting algorithm. For boundary layers, reasonably wide fitting plateaus could only be found for $Re_\tau \gtrsim 2000$, which was

TABLE I. Data sets used in the text.

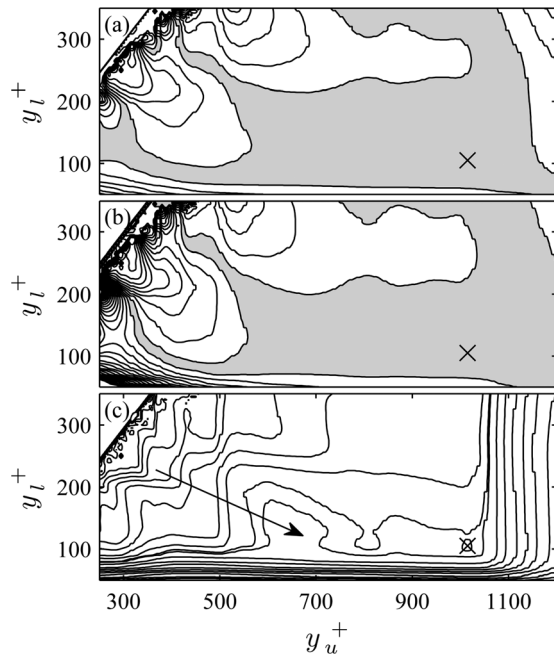| Reference | Flow | Method | $Re_\tau$ |
|---|---|---|---|
| P1 (Ref. 25) | Pipe | Numeric | 1142 |
| BL1 (Ref. 26), BL2 (Ref. 27) | Boundary layers | Experiment | 1480–8500 |
| BL3 (Ref. 28) | Boundary layer | Numeric | 690 |
| C1 (Ref. 29), C2 (Ref. 30) | Channel | Experiment | 1454–3945 |
| C3 (Ref. 7), C4 (Ref. 24) | Channel | Numeric | 934, 2003 |

FIG. 2. (a) Contours of the best fitting $\kappa$ in model (10), for the channel C4. The contour interval is 0.01, and the shaded area is $0.355 < \kappa < 0.365$. (b) Contours for $\Pi$, spaced by 0.02, and shaded in $0.195 < \Pi < 0.215$. (c) Resulting error $S$. The contours are cubically spaced, starting from 0.008, and increasing in the direction of the arrow.
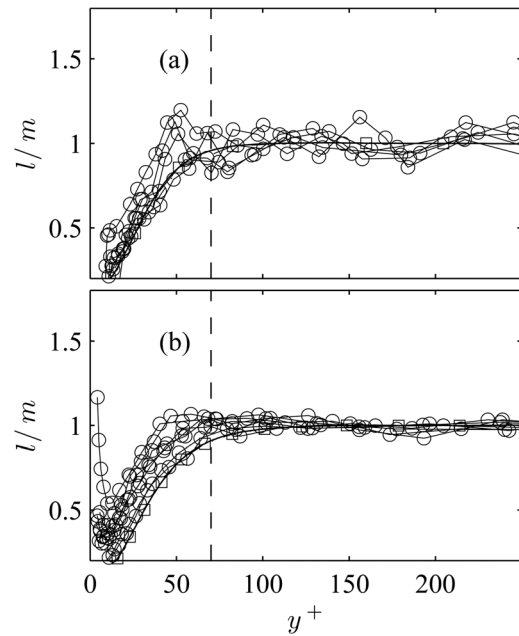


FIG. 3. Comparison of the mixing length $l(y)$ in Eq. (1) with the model $m(y)$ in Eq. (10), for (a) channels at $Re_\tau = 1454$, 1727, 2003, 2433, 3119, and 3945; (b) boundary layers at $Re_\tau = 1480$, 2330, 3260, 4140, 5300, 7060, and 8500, and pipe at $Re_\tau = 1142$. $\bigcirc$, experimental channels and boundary layers; $\square$, numerical channel C4 in (a) and pipe P1 in (b).

therefore taken to be the lowest Reynolds number for which an extended overlap region exists. The low-Reynolds number channel C3 and the boundary layer BL3 could only be fitted in a short range of $y$, and lacked the wide plateau of the $(y_l, y_u)$ sensitivity plots in Figs. 2(a) and 2(b).

Disregarding those very low Reynolds numbers, the lower and upper ends of the logarithmic region recovered by the model (10) scale in wall and outer units, respectively. The effect of the offset is to extend the lower end of the logarithmic region,[42] and Fig. 3 shows that our original estimate for the range of validity of the model was conservative, and that the actual fit is reasonably good above $y_b^+ \approx 70$ for all the data sets. The wake parameter $\Pi$ determines the upper end of the fit, which is seen in Fig. 4 to be $y_e/\delta = 0.5$ for internal flows and $y_e/\delta = 0.3$ for boundary layers.

The uncertainty of the estimated parameters stems not only from the errors in the original data, but also from the fitting procedure. We estimate it in the following way. Once the nominal values $\overline{\boldsymbol{q}}$ of the parameters are determined by fitting, and the bounds $y_b$ and $y_e$ of the model fit are defined by some comparison, such as those in Figs. 3 and 4, the nominal error of the model $m(y; \boldsymbol{q})$ with respect to the data is calculated as

$$\overline{S} \equiv S(y_l = y_b, y_u = y_e; \overline{\boldsymbol{q}}).$$

The uncertainty range of a given parameter, such as $\kappa$, is defined as the range of values for which the fitting error is smaller than $\overline{S}$ when all the other parameters are kept fixed at their nominal values. For example, if the nominal fitting parameters for a given case are $\overline{\kappa}$, $\overline{\Pi}$, and $\overline{y}_{off}$, the uncertainty range for $\kappa$ is defined as all those $\hat{\kappa}$ for which

$$S(y_b, y_e; \hat{\kappa}, \overline{y}_{off}, \overline{\Pi}) < \overline{S}. \tag{11}$$

Using the limits $(y_b^+, y_e/\delta)$ indicated in Figs. 3 and 4 to estimate the uncertainties, the results for $\kappa$ and $y_{off}$ are given in Figs. 5(a) and 5(b). The numerical data generally have lower uncertainties than the experimental ones. Both $\kappa$ and $y_{off}$ approach asymptotic values for large Reynolds numbers, as predicted by the theory, but their precise asymptotes can only be determined approximately by extrapolation. The Reynolds number dependence of the different model parameters is approximated in Fig. 5 by functions of the type $\alpha Re_\tau^{-1} + \beta$, as suggested by Eq. (5), and the "recommended"
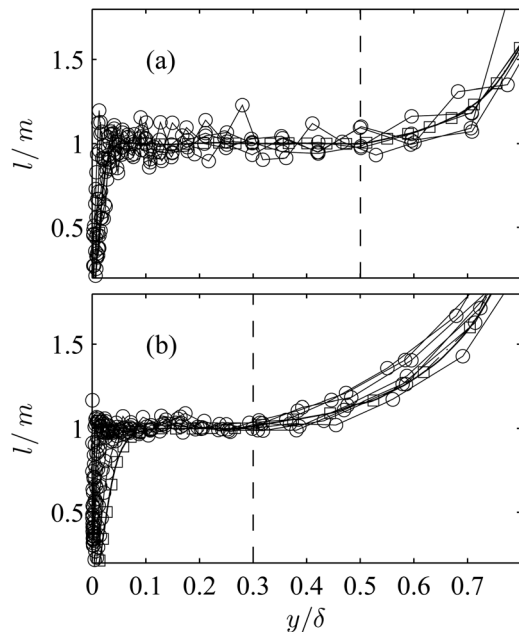


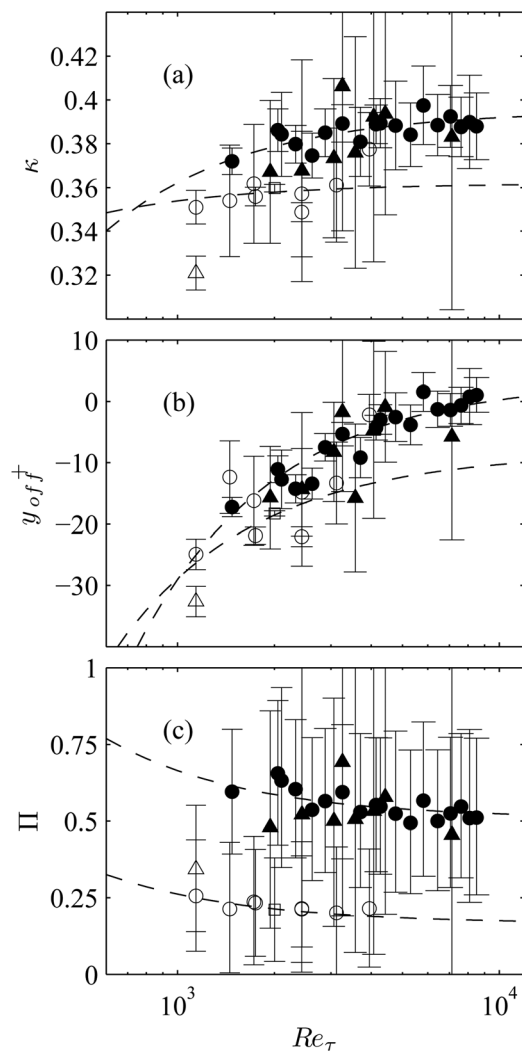FIG. 4. Same as Fig. 3, in outer units.

FIG. 5. Estimated parameters for the model (10), as functions of $Re_\tau$. (a) $\kappa$, (b) $y_{off}$, and (c) $\Pi$. ▲, BL1; ●, BL2; □, C4; ○, C1 and C2; △, P1. The dashed lines are approximations of the form $\beta + \alpha/Re_\tau$, with the parameters in Table 2.

coefficients for the three parameters are given in Table II. Their asymptotic values for large $Re_\tau$ are given by $\beta$.

The $\kappa$'s of the channels are lower than those of the boundary layers for all the available cases, and the asymptotes of the two flows are qualitatively similar, although not identical, to the commonly accepted values for boundary layers, $\kappa \approx 0.385$,[43,44] and channels $\kappa \approx 0.37$.[45] There is probably no reason why our analysis should agree exactly with the older ones. All of them, including ours, are in essence empirical fits using models optimized for different ranges of the Reynolds number. The present analysis is

TABLE II. Coefficients of the best fits of the parameters of the model (10) to a Reynolds number dependence of the form $\beta + \alpha/Re_\tau$.

|  | Boundary layers | | Channels | |
|---|---|---|---|---|
|  | $\alpha$ | $\beta$ | $\alpha$ | $\beta$ |
| $\kappa$ | −32.1 | 0.395 | −10.3 | 0.365 |
| $y_{off}$ | $-3.6 \times 10^4$ | 3.8 | $-2.0 \times 10^4$ | −8.5 |
| $\Pi$ | 185 | 0.51 | 96.4 | 0.16 |

mostly concerned with relatively low Reynolds numbers in the overlap layer, and the three references cited above center on the full velocity profile at high Reynolds numbers. However, the conclusion that the Kármán constant in channels is slightly lower than in boundary layers is common to both approaches, and should probably be taken as qualitatively correct.

The offset $y_{off}$ is negative in almost all the cases, and approaches zero as the Reynolds number increases. It represents the inner correction to Eq. (2), and the better scaling with $l(y)$ of the spectra in Fig. 1 can mostly be attributed to it. Fig. 5(b) suggests that its effect is still significant at $Re_\tau = O(10^3)$.

The wake parameter $\Pi$ is shown in Fig. 5(c). It represents the outer correction and extends the upper limit of the fit to a height independent of the Reynolds number. It is different for channels and boundary layers, in agreement with the well-known difference between their wake strengths, but each case is relatively independent of the Reynolds number. That gives some confidence in the adequacy of the linear term in Eq. (6) as a model for the effect of the wake on the logarithmic region, and it is reassuring that the asymptotic value of $\Pi$ given in Table 2 for boundary layers is comparable to the commonly accepted value of about 0.5.[44]

Equation (6) is not the only possible representation of the effect of the wake, and we tested models with no correction or with a constant leading correction to the velocity gradient. The linear choice discussed above, besides agreeing with the traditional approximation, was found to be less sensitive to the Reynolds number and to the details of the matching procedure. The useful ranges of $y$ and $Re_\tau$ can be further extended by models including more terms in the Laurent series expansion in Eq. (5), or by using different functional forms.[36,42]

## III. LENGTH-SCALES OF THE FLUCTUATIONS

### A. Wall-parallel scales

From the point of view of the rest of this paper, the main result in Sec. II is that the higher-order expansion of the mean velocity gradient in Fig. 6 defines an overlap region that is wider than the classical logarithmic approximation, as well as Reynolds-number independent. The inner limit, $y^+ = 70$, is common to internal and external flows, and the outer one is $y/\delta = 0.3$ for boundary layers and $y/\delta = 0.5$ for internal flows, most probably, because the stronger wake of the former would require more careful modeling. Fig. 6 shows that, even within those limited ranges, the mixing length differs appreciable from the linear behavior, specially for boundary layers at moderate Reynolds numbers. To reduce clutter, that figure is drawn with the model $m(y)$, but we have also included the actual mixing lengths for our two lowest-Reynolds-number flows: the channel C3 used in Figure 1 and the boundary layer BL3 with the even lower $Re_\tau = 690$. Neither is within the range of applicability of the model discussed in Sec. II, and neither can claim an asymptotic overlap range. However, we saw in Figure 1 that the mixing length is much better than $y$ as a scale for the velocity spectra of C3, and Figure 7 shows that the same is true for BL3.

In both cases, the scaling is restricted to the "core" regions marked by dashed rectangles in both figures, which
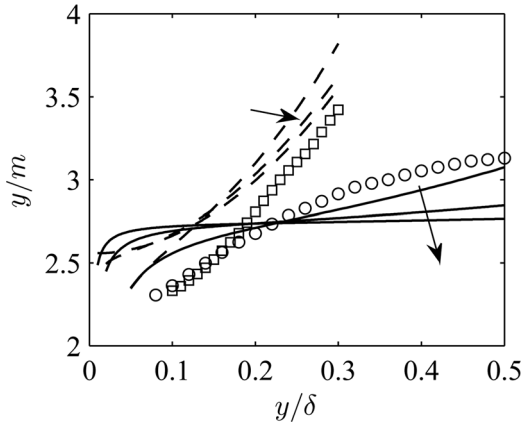
FIG. 6. Comparison of the mixing-length model $m(y)$ with the wall distance, using the values in Table 2. ——, channels; — —, boundary layers. $Re_\tau = 2000, 5000, 10\,000$, with the Reynolds number increasing in the direction of the arrows. Symbols are $l(y)$ for: ○, C3; □, BL3.

contain most of the spectral energy. Those ranges are insensitive to the Reynolds number and to the flow geometry, but they are different for each velocity component.[7] The cores of $\phi_{uu}$ and $\phi_{uv}$ are elongated in the streamwise direction, while those of $\phi_{vv}$ and $\phi_{ww}$ are more isotropic. We define them here as

$$\mathcal{L}_{uu} = \{5 < \lambda_x/l(y) < 50,\ 2.5 < \lambda_z/l(y) < 25\}, \quad (12)$$
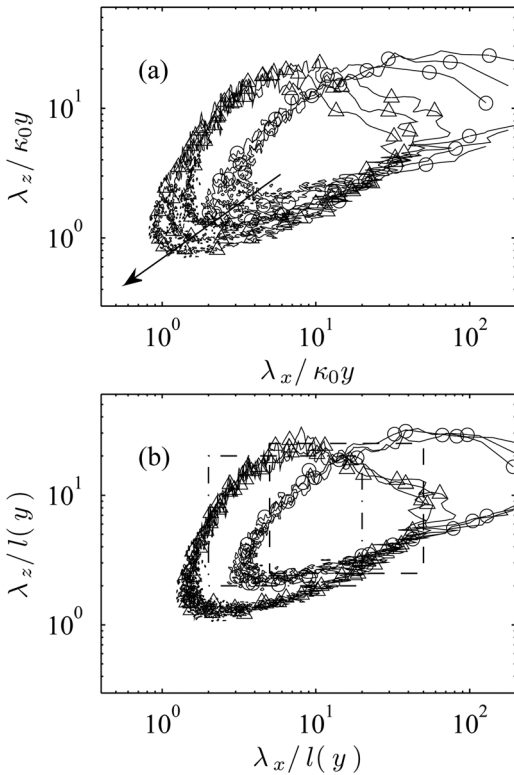


FIG. 7. Premultiplied two-dimensional spectra of the velocity fluctuations, as functions of the wavelengths for the boundary layer BL3, at $Re_\tau = 690$. (a) Normalized with $\kappa_0 y$, where $\kappa_0 = 0.395$. (b) Normalized with $l(y)$ from Eq. (1). ○, $k_x k_z \phi_{uu}$; △, $k_x k_z \phi_{vv}$. Contours are 0.05 of the local mean-squared intensity of each component. Spectra at $y/\delta = 0.2, 0.3$, and 0.4, with the arrow in the direction of increasing $y$. The rectangles enclose the "core" ranges defined in: — —, Eq. (12) for $u$, — · —, Eq. (13) for $v$.

for $u$, and

$$\mathcal{L}_{vv} = \{2 < \lambda_x/l(y) < 20,\ 2 < \lambda_z/l(y) < 20\}, \quad (13)$$

for $v$. The one-dimensional core spectra are defined as

$$
\begin{aligned}
E_{uu}^S(y, \lambda_z) &\equiv \int_{5 < \lambda_x/l(y) < 50} \phi_{uu}(y)\, \mathrm{d}k_x, \\
E_{vv}^S(y, \lambda_z) &\equiv \int_{2 < \lambda_x/l(y) < 20} \phi_{vv}(y)\, \mathrm{d}k_x,
\end{aligned}
\quad (14)
$$

and are shown in Fig. 8, normalized by their peak values to emphasize the scaling of their wavenumbers. The spectra of the streamwise fluctuation for different heights and different Reynolds numbers collapse well through the whole range of $\lambda_z$, and the channels agree reasonably well with the boundary layer. Note that Fig. 6 implies that, if the boundary layers and channels agree when scaled with $l(y)$, they should disagree when scaled with $y$. That seems to contradict Figure 10 in Ref. 28, where it was shown that the cores of the two-dimensional spectra of $u$ in C3 and BL3 agree well at $y/\delta = 0.3$. In fact, the difference is too small to be appreciated either in that paper or in Fig. 8. Even if the ratio $l(y)/y$ changes by about 30% over the overlap range, the maximum ratio between the $l(y)$ of BL3 and C3 at the same $y/\delta$ is only about 10% (Fig. 6).

The spectra of the wall-normal velocity also scale well with $l(y)$, except for the smallest scales, which begin to be contaminated by the isotropic inertial modes. The spectra of the spanwise velocity (not shown) collapse similarly well.

The evolution of the scaling with the distance to the wall is tested in Fig. 9, where the one-dimensional spectra of the streamwise velocity are plotted as functions of $\lambda_z/\delta$ and $y/\delta$. They are compared with isolines of $\lambda_z/l(y)$. The figure confirms that $l(y)$ captures well the behavior of the spectral length-scales of the core structures, and that the scaling extends over the overlap range defined in Sec. II for $y$. For the flows in Figs. 9(a) and 9(b), the growth of the length-scale with $y$ is slower than linear because of the influence from the inner and outer layers, but $l(y)$ describes those effects well. For the higher-Reynolds-number channel C4 in Fig. 9(c), the growth of the length-scale is much closer to linear, and both $y$ and $l(y)$ are reasonable scales.

### B. Wall-normal scales

The wall-normal length-scales of the fluctuations are measured by the two-point correlation function between $y$ and $y'$,

$$C_{\zeta\zeta}(y, y') \equiv \frac{\langle \zeta(y')\zeta(y) \rangle}{\langle \zeta(y')\zeta(y') \rangle}, \quad (15)$$

where $\zeta$ is an arbitrary velocity component. Townsend's hypothesis would predict that $C_{\zeta\zeta}$ is a function of $(y - y')/y'$, independently of $y'$, although Ref. 5 found that, in a pipe at $Re_\tau \simeq 2500$, the linear scaling only holds for the correlation of $u$ at moderate streamwise length-scales. We also restrict ourselves to correlations defined over the core wavelengths defined in Eqs. (12) and (13),
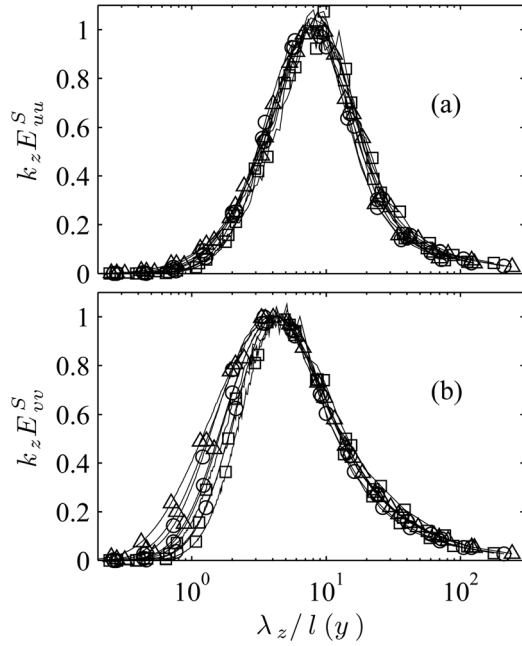
FIG. 8. Premultiplied "core" one-dimensional spectra of velocity fluctuations, as in Eq. (14). (a) $k_z E_{uu}^S(y, \lambda_z)$. (b) $k_z E_{vv}^S(y, \lambda_z)$, normalized by their individual maximum values, as functions of $\lambda_z/l(y)$. □, BL3; ○, C3; △, C4. Each case is shown at $y/\delta = 0.1, 0.2,$ and $0.4$.

$$C_{\zeta\zeta}^S(y, y') \equiv \frac{\int_{\mathcal{L}_{\zeta\zeta}} \psi_{\zeta\zeta}(y, y', \lambda_x, \lambda_z) \, dk_x \, dk_z}{\int_{\mathcal{L}_{\zeta\zeta}} \psi_{\zeta\zeta}(y', y', \lambda_x, \lambda_z) \, dk_x \, dk_z}, \qquad (16)$$

where

$$\psi_{\zeta\zeta}(y, y', \lambda_x, \lambda_z) \equiv \Re\left\{ \langle \hat{\zeta}(y', \lambda_x, \lambda_z) \hat{\zeta}^*(y, \lambda_x, \lambda_z) \rangle \right\},$$

and $\mathcal{R}$ represents the real part. For large separations in $y$, the correlation length cannot be associated with either $y$ or $y'$, and we use length-scales based on thresholding the correlation at different levels,

$$\Lambda_{\zeta\zeta}^{+(-)}(y', \sigma) \equiv y - y', \qquad (17)$$

where $y > (<) y'$ satisfies

$$C_{\zeta\zeta}^S(y, y') = \sigma.$$

By definition, $\Lambda^+$ and $\Lambda^-$ are, respectively, always positive and negative. The definition of these lengths is illustrated in Fig. 10. We test their scaling with respect to length-scales evaluated at the mid point, $y_m^\pm = y' + \Lambda^\pm/2$, between $y$ and $y'$.

Figure 11 shows $\Lambda_{uu}^\pm$ and $\Lambda_{vv}^\pm$ normalized by $\kappa_0 y_m^\pm$ and by $l(y_m^\pm)$, and it is clear that they scale better with the mixing length than with the wall distance. The scaling works up to $y' \approx 0.4\delta$, which is comparable to the scaling range for the spectra in Fig. 9(b). The correlation length of $w$ behaves similarly. The scaling breaks down near the center of the channel, in part because $\Lambda^\pm$ begins to be comparable to $\delta$, and the reference point $y_m^\pm$ moves too far from either $y$ or $y'$ to expect any single wall distance to represent the full correlation length. For example, $l(y)$ diverges at the center of channel. In addition, the effect of the large scales still contained
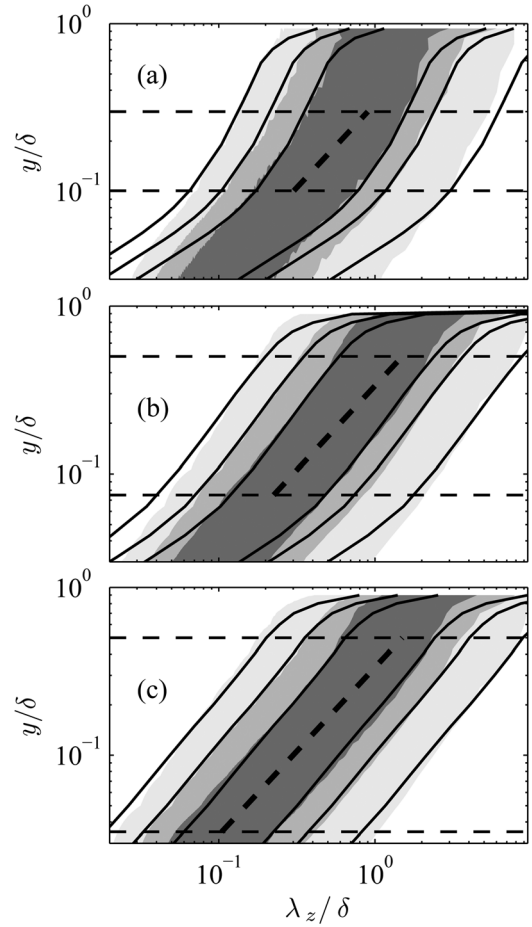


FIG. 9. Contours of premultiplied one-dimensional spectra $k_z E_{uu}^S(y, \lambda_z)$ for (a) BL3, (b) C3, and (c) C4, normalized by the intensity at each height, as functions of $\lambda_z/\delta$ and $y/\delta$. Contour-levels are at 0.05, 0.15, and 0.3. Horizontal dashed lines are the overlap range, $y^+ = 70$ to $y/\delta = 0.3$ in (a), and 0.5 in (b) and (c). Solid curves are defined by $\lambda_z/l(y) = const.$ placed to align with the contours. The dashed diagonal is linear scaling.

within the core rectangles becomes stronger near the centerline. If $\mathcal{L}_{uu}$ or $\mathcal{L}_{vv}$ is made narrower, the well-scaled range becomes longer, whereas the full correlation functions in Eq. (15), which include all the large scales, scale much worse than those in Fig. 11. That is particularly true for $C_{uu}$, while the correlations of the cross-stream velocities, $C_{vv}$ and $C_{ww}$, which have weaker large-scale contributions, scale comparatively better.

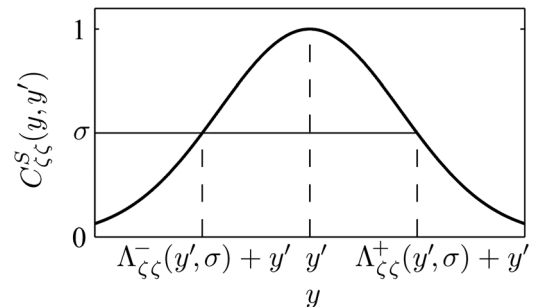We have also examined the numerical channel at $Re_\tau = 550$ from Ref. 7, which was not included in the



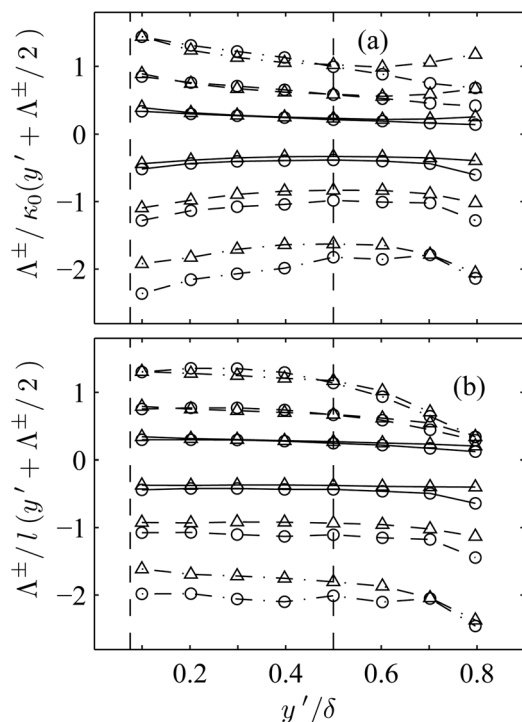FIG. 10. Schematic plot of wall-normal length-scale of fluctuations defined by Eq. (17).

FIG. 11. Correlation lengths $\Lambda^{\pm}(y', \sigma)$ defined by Eq. (17) for: ——, $\sigma = 0.9$; — —, 0.6; — · —, 0.3. Channel C3, normalized with (a) $\kappa_0(y_m^{\pm})$ and (b) $l(y_m^{\pm})$. ◯, $\Lambda_{uu}^{\pm}$; △, $\Lambda_{vv}^{\pm}$. The vertical dashed lines are $y'^+ = 70$ and $y'/\delta = 0.5$.

## IV. CONCLUSIONS

We have shown that the overlap range of the mean velocity profile in turbulent pipes, channels, and boundary layers can be extended to a wider range of wall distances by including terms of $O(Re_\tau^{-1})$ in its asymptotic expansion. That agrees with previous results by other authors, but the approximation used here is optimized for relatively low Reynolds numbers, in which there are substantial differences among models of the overlap region that can be used to test different scaling hypotheses. By comparing with numerical and experimental data, the overlap obtained from our model is shown to extend from $y^+ = 70$ to $y/\delta = 0.3$ in boundary layers, and to $y/\delta = 0.5$ in internal flows.

The expansion holds at much lower Reynolds numbers, $Re_\tau \approx 600$,[36] than the lowest-order traditional logarithmic law, and allows us to define a "mixing" length, $l(y) = (dU^+/dy)^{-1}$, that incorporates some of the effects of viscosity and of the flow thickness. For $Re_\tau \lesssim 1000$, the differences between $l(y)$ and the $y$ are substantial, specially in boundary layers, and we use them to test whether the length scale of the velocity fluctuations is best described by the distance to the wall, or by the local shear.

It turns out that the latter is the better scaling. There is a "core" region of the two-dimensional wall-parallel velocity spectra, defined by wavelengths of $O(y)$, which scales much

better with $l(y)$ than with $y$. As expected, neither the smaller inertial eddies, nor the very-large ones with wavelengths of $O(\delta)$ scale with $y$ or with $l(y)$. When the wall-normal correlation functions of the three velocity components are compiled over those core wavelengths, they also scale better with $l(y)$ than with $y$. Even if $l(y)$ approaches $y$ as $Re_\tau \to \infty$, we have shown that they are still visibly different in boundary layers at $Re_\tau \approx 10^4$. It is interesting to speculate about what those observations might mean for the dynamics of the attached active eddies of wall-bounded turbulence. The correction that is most effective in extending the overlap region is the virtual origin, which describes how the mean profile "sees" the wall, although the wake correction also helps. What the scaling results show is that the mean velocity and the fluctuations see the wall at the same location. The implied model is slightly different from the traditional one, suggesting that the structures are not controlled by their geometry with respect to the wall, but by the local shear, or time scale, of the velocity profile.

A serendipitous application of the present results is that an effective logarithmic range can be most easily identified in low-Reynolds-number experiments or simulations by searching for a linear behavior of the mixing time $(dU/dy)^{-1}$, rather than by using the indicator $(ydU^+/dy)^{-1}$, since the former is insensitive both to an additive constant, and to a virtual origin. For example, that could be useful in analyzing flows over rough walls.

[1]C. B. Millikan, "A critical discussion of turbulent flows in channels and circular tubes," in *Proceedings of the 5th International Conference on Applied Mechanics* (Wiley, New York, 1938), pp. 386–392.
[2]A. A. Townsend, *The Structure of Turbulent Shear Flows*, 2nd ed. (Cambridge University Press, Cambridge, 1976).
[3]A. A. Townsend, "Equilibrium layers and wall turbulence," J. Fluid Mech. **11**, 97 (1961).
[4]A. E. Perry and C. J. Abell, "Scaling laws for pipe-flow turbulence," J. Fluid Mech. **67**, 257 (1975).
[5]K. J. Bullock, R. E. Cooper, and F. H. Abernathy, "Structural similarity in radial correlations and spectra of longitudinal velocity fluctuations in pipe flow," J. Fluid Mech. **88**, 585 (1978).
[6]D. B. deGraaff and J. K. Eaton, "Reynolds number scaling of the flat-plate turbulent boundary layer," J. Fluid Mech. **422**, 319 (2000).
[7]J. C. delÁlamo, J. Jiménez, P. Zandonade, and R. D. Moser, "Scaling of the energy spectra of turbulent channels," J. Fluid Mech. **500**, 135 (2004).
[8]K. C. Kim and R. J. Adrian, "Very large-scale motions in the outer layer," Phys. Fluids **11**, 417 (1999).
[9]M. Guala, S. E. Hommema, and R. J. Adrian, "Large-scale and very-large-scale motions in turbulent pipe flow," J. Fluid Mech. **554**, 521 (2006).
[10]S. C. C. Bailey, M. Hultmark, A. J. Smits, and M. P. Schultz, "Azimuthal structure of turbulence in high Reynolds number pipe flow," J. Fluid Mech. **615**, 121 (2008).
[11]J. C. delÁlamo, J. Jiménez, P. Zandonade, and R. D. Moser, "Self-similar vortex clusters in the turbulent logarithmic region," J. Fluid Mech. **561**, 329 (2006).
[12]J. P. Monty, J. A. Stewart, R. C. Williams, and M. S. Chong, "Large-scale features in turbulent pipe and channel flows," J. Fluid Mech. **589**, 147 (2007).

[13]C. D. Tomkins and R. J. Adrian, "Spanwise structure and scale growth in turbulent boundary layers," J. Fluid Mech. **490**, 37 (2003).

[14]O. Flores and J. Jiménez, "Effect of wall-boundary disturbances on turbulent channel flows," J. Fluid Mech. **566**, 357 (2006).

[15]J. C. R. Hunt, P. Moin, R. D. Moser, and P. R. Spalart, "Self similarity of two point correlations in wall bounded turbulent flows," CTR Annu. Res. Briefs **1987**, 25 (1987).

[16]J. Jiménez, "The largest scales of turbulent wall flows," CTR Annu. Res. Briefs **1998**, 137 (1998).

[17]J. Jiménez and S. Hoyas, "Turbulent fluctuations above the buffer layer of wall-bounded flows," J. Fluid Mech. **611**, 215 (2008).

[18]P. S. Jackson, "On the displacement height in the logarithmic velocity profile," J. Fluid Mech. **111**, 15 (1981).

[19]W. J. Duncan, A. S. Thom, and A. D. Young, *Mechanics of Fluids*, 2nd ed. Arnold, London, 1970.

[20]M. Oberlack, "Unified approach for symmetries in plane parallel shear flows," J. Fluid Mech. **427**, 299 (2001).

[21]M. Wosnik, L. Castillo, and W. K. George, "A theory for turbulent pipe and channel flows," J. Fluid Mech. **421**, 115 (2000).

[22]P. R. Spalart, G. N. Coleman, and R. Johnstone, "Direct numerical simulation of the Ekman layer: A step in Reynolds number, and cautious support for a log law with a shifted origin," Phys. Fluids **20**, 101507 (2008).

[23]M. H. Buschmann and M. Gad-el-Hak, "New mixing-length approach for the mean velocity profile of turbulent boundary layers," ASME J. Fluids Eng. **127**, 393 (2005).

[24]S. Hoyas and J. Jiménez, "Scaling of the velocity fluctuations in turbulent channels up to $Re_\tau = 2003$," Phys. Fluids **18**, 011702 (2006).

[25]X. Wu and P. Moin, "A direct numerical simulation study on the mean velocity characteristics in turbulent pipe flow," J. Fluid Mech. **608**, 81 (2009).

[26]M. H. Hites, "Scaling of high-Reynolds number turbulent boundary layers in the National Diagnostic Facility," Ph.D. dissertation (Illinois Institute of Technology, Illinois, 1997).

[27]J. M. Österlund, "Experimental studies of zero-pressure gradient turbulent boundary-layer flow," Ph.D. dissertation (Royal Institute of Technology, Stockholm, 1999).

[28]J. Jiménes, S. Hoyas, M. P. Simens, and Y. Mizuno, "Turbulent boundary layers and channels at moderate Reynolds numbers," J. Fluid Mech. **657**, 335 (2010).

[29]K. T. Christensen and R. J. Adrian, "Statistical evidence of hairpin vortex packets in wall turbulence," J. Fluid Mech. **431**, 433 (2001).

[30]J. P. Monty, "Developments in smooth wall turbulent duct flows," Ph.D. dissertation (The University of Melbourne, Melbourne, 2005).

[31]D. Coles, "The law of the wake in the turbulent boundary layer," J. Fluid Mech. **1**, 191 (1956).

[32]U. Piomelli, "Wall-layer models for large-eddy simulations," Prog. Aerosp. Sci. **44**, 437 (2008).

[33]M. van Dyke, *Perturbation Methods in Fluid Mechanics*, 2nd ed. (The Parabolic, Stanford, 1975).

[34]N. Afzal and K. Yajnik, "Analysis of turbulent pipe and channel flows at moderately large Reynolds number," J. Fluid Mech. **61**, 23 (1973).

[35]J. Jiménez and R. D. Moser, "What are we learning from simulating wall turbulence?," Philos. Trans. R. Soc. A **365**, 715 (2007).

[36]M. H. Buschmann and M. Gad-el-Hak, "Evidence of nonlogarithmic behavior of turbulent channel and pipe flow," AIAA J. **47**, 535 (2009).

[37]M. H. Buschmann and M. Gad-el-Hak, "Generalized logarithmic law and its consequences," AIAA J. **41**, 40 (2003).

[38]T. S. Lundgren, "Asymptotic analysis of the constant pressure turbulent boundary layer," Phys. Fluids **19**, 055105 (2007).

[39]A. K. Lewkowicz, "An improved universal wake function for turbulent boundary layers and some of its consequences," Z. Flugwiss. Weltraumforsch. **6**, 261 (1982).

[40]M. H. Buschmann and M. Gad-el-Hak, "Recent developments in scaling of wall-bounded flows," Prog. Aerosp. Sci. **42**, 419 (2007).

[41]W. H. Press, S. A. Teukolsky, W. T. Vetterling, and B. P. Flannery, *Numerical Recipes. The Art of Scientific Computing*, 3rd ed. (Cambridge University Press, Cambridge, 2007), pp. 801–806.

[42]B. Lindgren, J. M. Österlund, and A. V. Johansson, "Evaluation of scaling laws derived from Lie group symmetry methods in zero-pressure-gradient turbulent boundary layers," J. Fluid Mech. **502**, 127 (2004).

[43]J. Österlund, A. Johansson, H. Nagib, and M. Hites, "A note on the overlap region in turbulent boundary layers," Phys. Fluids **12**, 1 (2000).

[44]H. M. Nagib, K. A. Chauhan, and P. A. Monkewitz, "Approach to an asymptotic state for zero pressure gradient turbulent boundary layers," Philos. Trans. R. Soc. A **365**, 755 (2007).

[45]E. S. Zanoun, F. Durst, and H. Nagib, "Evaluating the law of the wall in two-dimensional fully developed turbulent channel flows," Phys. Fluids **15**, 3079 (2003).